# Simulating the Effects of the Addition of a Large Area GEM at a Detector for a Future Electron Ion Collider

Undergraduate Research Report by Akshath Wikramanayake
Research Advisor: Dr. Marcus Hohlmann

***Abstract*—The effect of the addition of a large area GEM detector to the far forward region of the proposed Brookhaven eA Solenoidal Tracker (BeAST) was studied by simulating the detector using the EicRoot framework. The impact of the large area GEMs was studied as a function of particle scattering angle and particle momentum. The results suggest that the addition of a large area GEM can significantly improve the momentum resolution of the BeAST detector.**

## I. Background and Detector Geometry

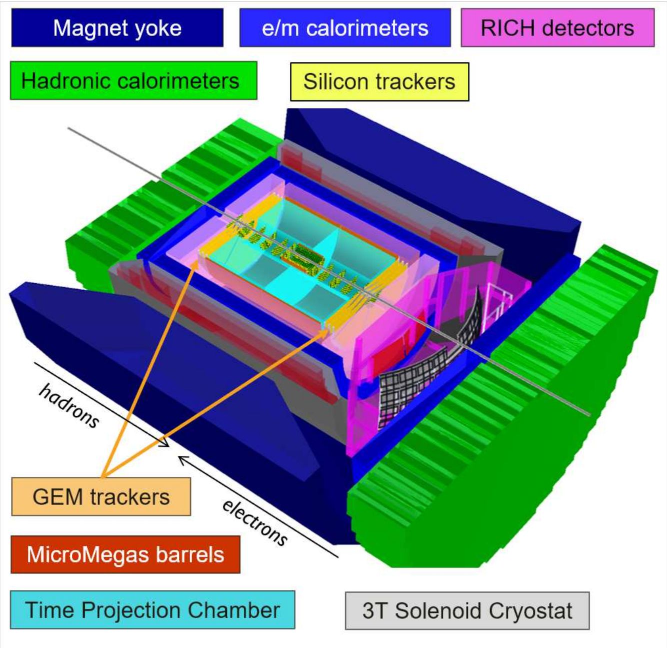


Fig. 1. The current working geometry of the BeAST detector with the major components labeled. [1]

The Brookhaven eA Solenoidal Tracker (BeAST) is a prototype detector that is currently being designed by the Brookhaven National Laboratory to potentially be used at the proposed Electron Ion Collider. One proposed change to the current working design of the BeAST detector is the addition of a large area GEM detector to the far-forward region of the BeAST detector.

In order to study the effect of the addition of this large area GEM (henceforth referred to as an ”outer GEM”) to the overall resolution, the BeAST detector was simulated in two configurations using the EicRoot framework: a control geometry intended to replicate the current working BeAST detector geometry, and a test geometry that included an added outer GEM detector in addition to all the components of the control geometry.

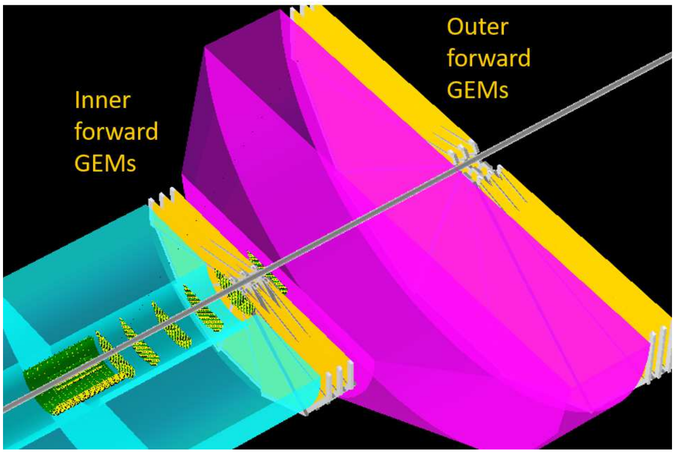


Fig. 2. The simulated test geometry as seen in the EicRoot event display.

Figure 1 shows a schematic of the current working geometry of the BeAST detector. The current simulated geometry in EicRoot is only a partial approximate reconstruction of this detector geometry. The simulated detector components for the control geometry include the beampipe, the Silicon and Vertex tracers, the GEM detectors (which are shown in figure 1, henceforth referred to as ”inner GEM” detectors), the time projection chamber, and the ring imaging Cherenkov (RICH) detector gas volume. The test geometry includes additional outer GEM detectors in addition to all the components of the control geometry listed above. Figure 2 is a screenshot of the simulated detector obtained using the EicRoot event display, which shows the intended position of the outer GEM detector.

The impact of the outer GEM detector on the overall performance of the BeAST detector was studied by simulating the performance of the BeAST detector in the control and test configurations while varying the test particle parameters (scattering angle and momentum). By doing this, the effect of the outer GEMs was measured separately as a function of scattering angle and momentum. For the purposes of simulation, it was assumed that the detector would operate with a 1.5 Tesla B-field.

## II. Momentum Resolution

The basic process by which EicRoot simulates the performance of a detector is as follows. EicRoot first simulates the detector geometry with all other detector parameters such as the B-field. Then, the framework simulates particle hits with given parameters such as scattering angle and momentum. Each trial henceforth (i.e, each data point o a graph) was conducted with 1000 simulated particle tracks. EicRoot then attempts to reconstruct the particle track data using the hits created by the detector components. The accuracy and precision of the reconstructed particle tracks can be used to quantify the performance of the detector. This can be done by examining the momentum uncertainty, defined by the equation:

$$\frac{P_{\text{reconstruction}} - P_{\text{simulation}}}{P_{\text{simulation}}} \ [\%]$$

The momentum resolution for a given trial is obtained by taking the mean of the histogram of momentum uncertainties for the 1000 simulated particle tracks. By applying a Gaussian fit to the histogram, the fit parameters were used to apply error bars to the momentum resolution.

## III. Momentum Resolution vs Scattering Angle

The effect of the outer GEMs as a function of the scattering angle of the test particles was studied by conducting simulations with the control and test geometries while varying the scattering angle. The scattering angle, $\theta$, was varied from 5° to 75°. As expected, the effect of the outer GEMs was confined to scattering angles less than approximately 35° (corresponding to a pseudorapidity of $\eta \rangle$ 1.154), corresponding to the angular size of the detector. Beyond this scattering angle, the particles no longer interact with the outer GEMs, and thus the control and test geometries operate with the same resolution. It should be noted that the dimensions of the outer GEMs in these simulations was chosen somewhat arbitrarily to approximately match the angular size of the inner GEMs. Thus the limiting value of 35° may be subject to change if the dimensions of the outer GEMs are altered.

The results of this trial are shown in figure 3. This plot shows the momentum resolution of the detector as a function of scattering angle, $\theta$. The aforementioned limiting angle of $\theta$ = approximately 35° is marked by the convergence of the two trendlines.

Figure 4 shows the same results cropped to focus on the region in which the outer GEMs affect momentum resolution.

from this graph (figure 4), it is clear that the outer GEMs provide a significant improvement to momentum resolution, particularly for small angles of deviation. The fine structure of the trendlines is believed to be due to the varying number of hits on the individual detectors. In order to verify this, another script was created to extract the data for the number of hits on each detector during each trial so that any possible correlation between the number of hits and the momentum resolution

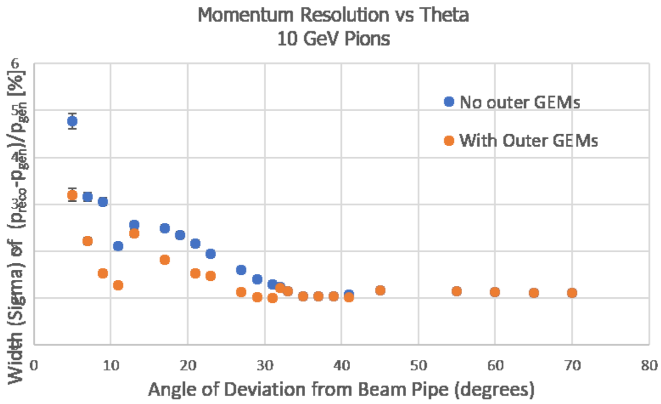


Fig. 3. Results of the test of Momentum Resolution vs Scattering Angle.

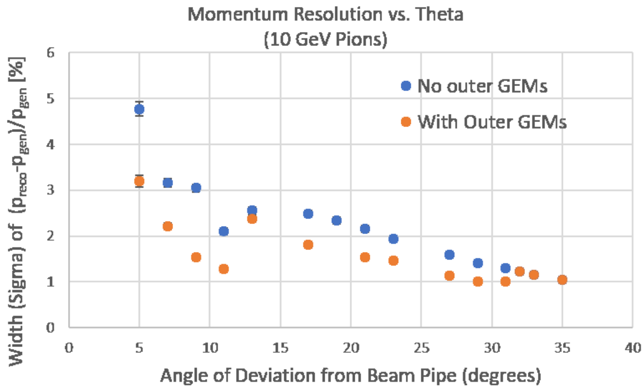


Fig. 4. Results of the test of Momentum Resolution vs Scattering Angle cropped to to show the region in which the outer GEM operates.

could be verified. The data showing the number of hits on each detector as a function of $\theta$ is produced in figure 5.

It is difficult to directly correlate the number of hits in the graph in figure 5 to the structure of the trendlines seen in figure 3 due to the large amount of data contained in the former. For clarity, it is beneficial to break figure 5 into three regions: small, intermediate, and large angles. For simplicity, let us examine the large $\theta$ region first, as only two detectors are active in this region: The Vertex tracker and the TPC. The momentum resolution distribution and the number of hits on the active detectors in this region (the TPC and the Vertex tracker) are shown in figure 6.

Although the variations in the momentum resolution graph appear exaggerated as the y-axis range is small, it is clear that both distributions are roughly linear. Furthermore, the local maximum of the top distribution (corresponding to a local minimum in resolution) corresponds to a local minimum in the number of hits produced by the Vertex tracker. If it is assumed that the EicRoot framework weighs Vertex tracker hits more heavily than TPC hits (which is likely, or else the TPC would completely dominate above mid-range $\theta$ values), then the distribution of the number of hits explains the momentum resolution distribution well.

Performing a similar analysis for mid-range values of $\theta$ is

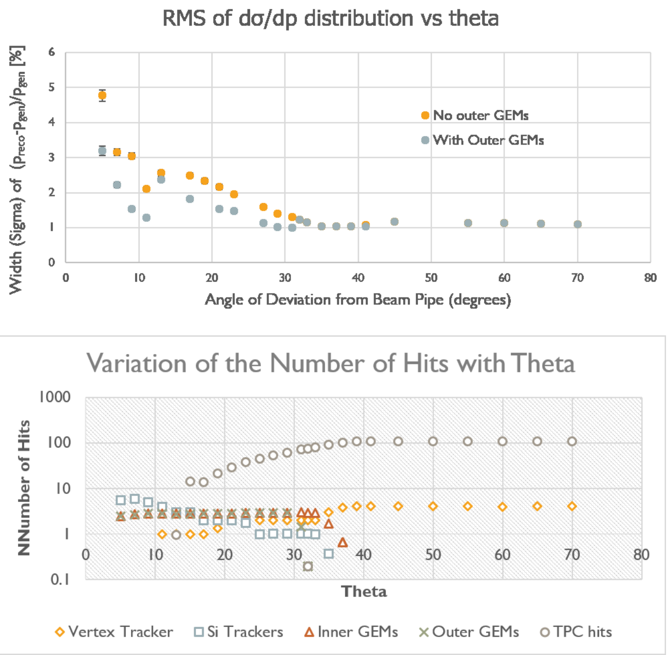


Fig. 5. Top: Momentum Resultion Uncertainty vs. Theta. Bottom: Number of hits on each detector vs. Theta.

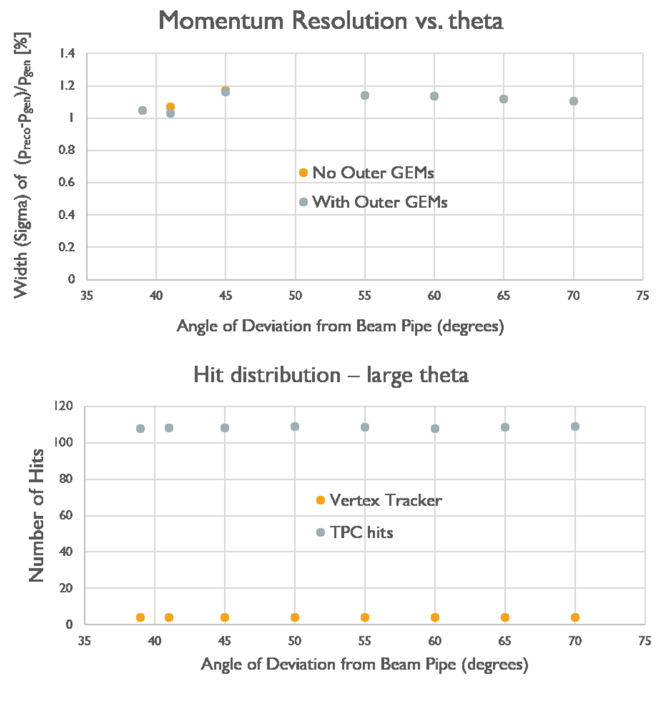


Fig. 6. Top: Momentum Resultion Uncertainty vs. Theta for large values of Theta. Bottom: Number of hits on each detector vs. Theta.

more challenging as all the detector components produce hits in this region. The results are produced in figure 7. However, there is a clear overall downward trend in the momentum uncertainty distribution at the top of figure 7 (meaning a steady overall improvement to momentum resolution) which corresponds to the rapid increase in the number of hits produced by the TPC (shown in the middle distribution). Furthermore, as expected, the trendlines for the distributions for the two geometries converge at the same angle at which the number of hits produced by the outer GEMs go to zero (marked by X's in the bottom distribution of figure 7).

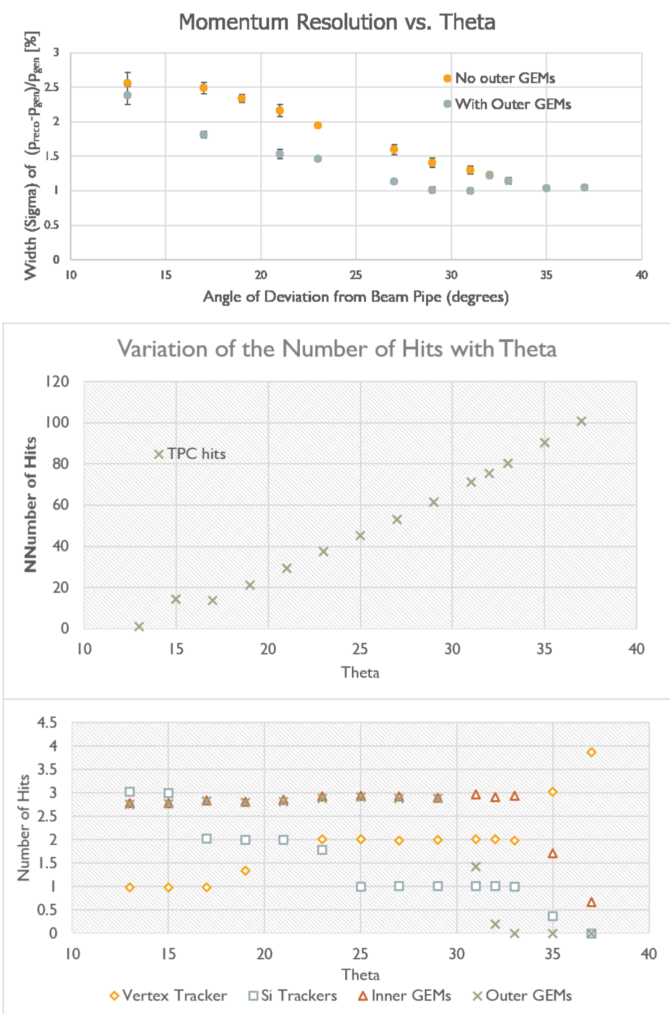


Fig. 7. Top: Momentum Resultion Uncertainty vs. Theta for mid-range values of Theta. Middle: Number of hits on the TPC vs. Theta. Bottom: Number of hits on the other detectors vs. Theta.

The final region to be examined is that of small values of $\theta$, shown in figure 8. For very low $\theta$ (5° to 9°), only the Silicon trackers produce hits. Here, there is a slight dip in the difference between the two distributions at 7°, which corresponds to a local maximum in the number of Si tracker hits. This may be because the jump in Si tracker hits means the relative dependence on the outer GEMs is reduced. The difference is reduced once again at 11°, which is when the Vertex tracker begins producing hits (which once again reduces the relative dependence on the outer GEMs). The difference between the two trends reaches a global minimum at 13°, which is when the TPC begins producing an appreciable number of hits in addition to the Si trackers.

Using the idea that the relative dependence on the outer GEMs should govern the difference between the momentum

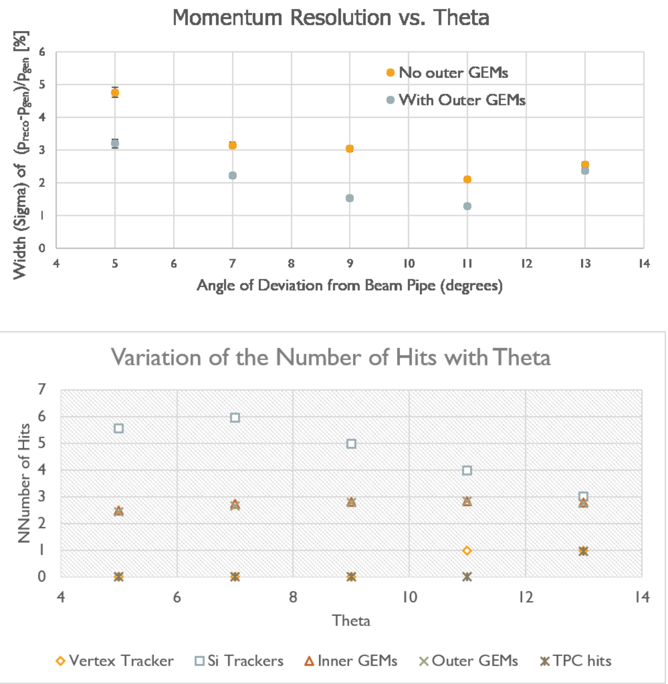


Fig. 8. Top: Momentum Resultion Uncertainty vs. Theta for small values of Theta. Bottom: Number of hits on the active detectors in this region vs. Theta.

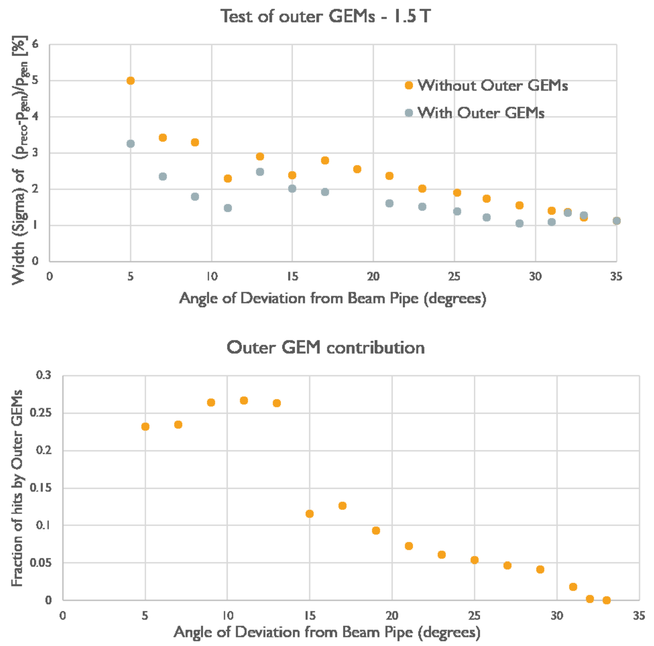


Fig. 9. Top: Momentum Resultion Uncertainty vs. Theta. Bottom: Fraction of hits on outer GEMs over total number of hits vs. Theta.

uncertainty trendlines for the two geometries, a plot of the fraction of outer GEM hits over the total number of hits was made and has been produced in figure 9. If hits on all components are considered to be equal (i.e., one TPC hit is weighted equally with one Si Tracker hit, or one GEM hit, and so on), then the gap between the distributions on the upper graph should be proportional to the corresponding value on the lower graph. There is some supporting evidence, such as large gaps in the upper graph for small $\theta$ values, and the distributions in the upper graph converging as the lower distribution goes to zero. However, there is some contradictory evidence, such as the upper distributions narrowing as the lower graph hits its maximum.

Finally it should be possible to correlate the overall momentum resolution to the total number of hits across all detectors. The momentum uncertainty distribution was compared to a plot of the total number of hits, shown in figure 10.

If hits on all components are considered to be equal (i.e., one TPC hit is weighted equally with one Si Tracker hit, or one GEM hit, and so on), then the distribution of the upper graph should be roughly proportional to the inverse of the orange distribution of the lower graph. There is a large downward trend in the upper distribution corresponding to the region in which the number of TPC hits rapidly increases ($13°$ to $30°$) which agrees with the hypothesis. After $30°$, the number of hits on the outer GEMs, Si Trackers, and Inner GEMs each go to zero in succession (as can be seen in figure 5, and is visible in the form of dips in the gray distribution), which compensates for the rise in the number of hits on the TPC. This leads to an increase in the momentum uncertainty despite the rise in the overall number of hits (Note that this only holds

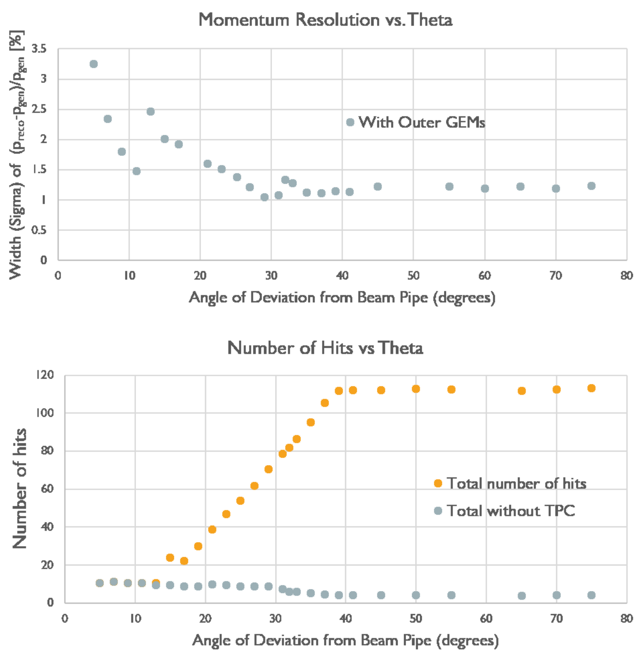


Fig. 10. Top: Momentum Resultion Uncertainty vs. Theta (test geometry). Bottom: Number of hits vs. Theta.

if it is assumed that the TPC hits are not weighted equally to hits on other detectors, which is justified based on the prior analysis for the fraction of outer GEM hits).

## IV. Momentum Resolution vs Particle Momentum

The momentum uncertainty of the detector was studied while keeping the scattering angle constant at $\theta$ = 15.41° ($\eta$ = 2.00) and varying the momentum of the simulated particles. The simulations were conducted for momentums ranging from 1 GeV/c to 60 GeV/c, which is believed to encompass the expected energy range for impinging particles at this portion of the BeAST detector [1]. The results are shown in figure 11.

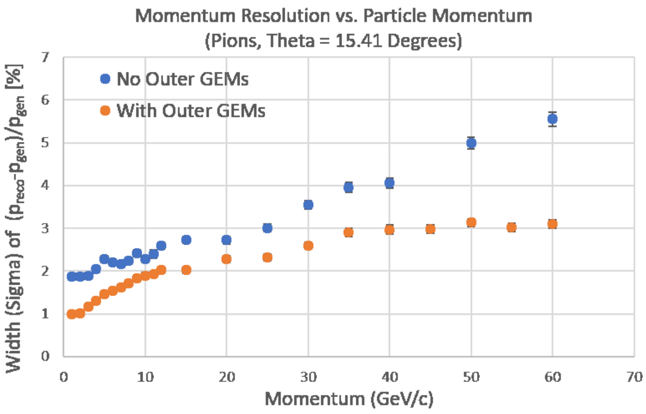


Fig. 11. Top: Momentum Resultion Uncertainty vs. Theta for large values of Theta. Bottom: Number of hits on each detector vs. Theta.

In addition to the two geometries at 1.5 Tesla, the test geometry was also considered at 3.0 Tesla to examine the extent of the effect of the outer GEMs (shown by the red distribution). The results show that the outer GEMs have a significant effect across the entire momentum range tested, but the improvement (signified by the gap between the orange and gray distributions) is particularly pronounced at the very low and very high momentum limits.

This result is particularly interesting because the prior momentum resolution vs scattering angle study was conducted with 10 GeV/c pions, where the improvement as seen in figure 11 is relatively small. This result may indicate that the improvement obtained by using the outer GEM detectors seen in the prior section may be even greater at other particle momentums.

## V. Project Outlook and Future Work

This analysis can be continued by performing the scattering angle analysis for other particle momentums, and the particle momentum analysis for other fixed scattering angles. This would provide a comprehensive map of the performance of the detector In the space of test particle parameters. However, the issues encountered with upgrading the EicRoot framework to store particle track parameters to potentially enable position resolution tracking have not been resolved.

Other members of the research group are experienced with using the EicRoot framework and could continue this analysis. The results of this study suggest that a large area GEM detector would be beneficial to the BeAST detector. As the EIC project already involves the construction of GEM detectors, it is hoped that this report might be beneficial towards guiding the scope of the EIC project at Florida Tech.

## References

[1] Alexander Kiselev. BeAST Detector. Argonne EIC User Group Meeting. 2016